Automatica 115 (2020) 108852

Contents lists available at ScienceDirect

Automatica

journal homepage: www.elsevier.com/locate/automatica

Torque and cadence tracking in functional electrical stimulation induced cycling using passivity-based spatial repetitive learning control ☆

Victor H. Duenas [a,*], Christian A. Cousin [b], Vahideh Ghanbari [c], Emily J. Fox [d], Warren E. Dixon [e]

[a] Department of Mechanical and Aerospace Engineering, Syracuse University, Syracuse, USA
[b] Department of Mechanical Engineering, University of Alabama, Tuscaloosa, USA
[c] Department of Electrical Engineering, University of Notre Dame, Notre Dame, USA
[d] Department of Physical Therapy, University of Florida, Gainesville, USA
[e] Department of Mechanical and Aerospace Engineering, University of Florida, Gainesville, USA

ARTICLE INFO

Article history:
Received 26 March 2018
Received in revised form 13 August 2019
Accepted 18 January 2020
Available online 7 February 2020

Keywords:
Functional Electrical Stimulation (FES)
FES-cycling
Spatial repetitive learning control (RLC)
Passivity-based control
Human–machine interaction

ABSTRACT

Due to the inherent periodic nature of cycling tasks, iterative and repetitive learning controllers are well motivated for rehabilitative cycling. Motorized functional electrical stimulation induced cycling is a rehabilitation treatment where multiple lower-limb muscle groups are activated jointly with an electric motor to achieve cycling objectives such as speed (cadence) and torque tracking. This paper examines torque tracking accomplished by the stimulation of six lower-limb muscles via a novel spatial repetitive learning control and cadence regulation by an electric motor using a sliding-mode controller. A desired torque trajectory is constructed based on the rider's kinematic efficiency, which is a function of the crank position. The learning controller takes advantage of the periodicity of the desired torque trajectory to provide a feedforward input to the stimulated muscles. A passivity-based analysis is developed to ensure stability of the torque and cadence closed-loop error systems. The muscle learning and electric motor controllers were implemented in real-time during cycling experiments on five able-bodied individuals and three participants with movement disorders. The combined average cadence tracking error was 0.01 ± 1.20 RPM for a 50 RPM trajectory and the combined average power tracking error was 1.78 ± 1.25 W for a peak power of 10 W.

1. Introduction

Functional Electrical Stimulation (FES) and robotic devices seek to enhance the quality of life of people with neurological conditions (NCs) by restoring mobility. Closed-loop FES control has been implemented in upper-limb tasks (Lew, Alavi, Randhawa, & Menon, 2016; Rouse, Duenas, Cousin, Parikh, & Dixon, 2018), locomotion using neuroprostheses (Alibeji, Kirsch, & Sharma, 2015, 2017; Ha, Murray, & Goldfarb, 2016; Nataraj, Audu, & Triolo, 2017), and lower-limb cycling (Bellman, Cheng, Downey, Hass, & Dixon, 2016; Bellman, Downey, Parikh, & Dixon, 2017). Motorized FES-cycling aims to produce a coordinated movement by artificially activating lower-limb muscles and engaging an electric motor to provide assistance as needed. FES-cycling studies have been found to provide neurological, movement, and sensory gains to people with spinal cord injury (SCI) and post stroke (Ferrante, Pedrocchi, Ferrigno, & Molteni, 2008; Sadowsky et al., 2013).

Cadence and power tracking objectives have been developed for cardiovascular and strength training in FES-cycling. In cadence tracking, a desired speed trajectory is tracked by muscles with or without motorized assistance. In power tracking, a torque trajectory is also tracked along with the speed trajectory. Robust closed-loop controllers leveraging high-gain or high-frequency techniques (e.g., sliding-mode control) have been used for cadence tracking in Bellman et al. (2016, 2017), Farhoud and Erfanian (2014), Hunt et al. (2004) and Kawai, Bellman,

☆ This research is supported in part by the National Science Foundation, USA Graduate Research Fellowship Program under Grant No. DGE-1315138 and AFOSR, USA award number FA9550-18-1-0109. Any opinions, findings, and conclusions or recommendations expressed in this material are those of the author(s) and do not necessarily reflect the views of the sponsoring agency. The material in this paper was partially presented at the 2018 American Control Conference, June 27–29, 2018, Milwaukee, WI, USA. This paper was recommended for publication in revised form by Associate Editor Yang Shi under the direction of Editor Thomas Parisini.

* Corresponding author.
E-mail addresses: vhduenas@syr.edu (V.H. Duenas), cacousin@eng.ua.edu (C.A. Cousin), vghanbar@nd.edu (V. Ghanbari), ejfox@phhp.ufl.edu (E.J. Fox), wdixon@ufl.edu (W.E. Dixon).

https://doi.org/10.1016/j.automatica.2020.108852

Downey, and Dixon (2019). However, motivation exists to maximize the torque output produced by the lower-limb muscles as a means to build muscle mass (Szecsi, Straube, & Fornusek, 2014). Hence, the concurrent objectives of cadence and torque tracking (i.e., power tracking) have been studied for motorized FES-cycling, where each control objective is assigned to the muscles or electric motor. Power tracking in FES-cycling has been investigated using linear feedback control (Hunt et al., 2004), higher-order sliding-mode control (Farhoud & Erfanian, 2014), a Lyapunov-based switched dwell-time analysis (Cousin, Duenas, Rouse, & Dixon, 2017), and a discrete-time analysis where the controller was updated once at the beginning of each crank cycle (Bellman, 2015). None of the aforementioned results exploit the repetitive/periodic nature of cycling to design learning-based controllers while guaranteeing the stability of the human-machine closed-loop system.

Since people undergoing movement therapy often have diminished torque producing capacity, an electric motor is typically used to assist FES-induced cycling. However, the use of an electric motor raises an additional concern for safe interaction between the rider and the motor. Motivated to ensure safe human–robot interaction, passivity theory has been used to design controllers in human applications including exercise machines and exoskeletons (Li & Horowitz, 1997; Zhang & Cheah, 2015). Closed-loop controllers that ensure passivity in the human–robot system are beneficial due to their compliant behavior, which also yield safe performance (Zhang & Cheah, 2015). In this paper, passivity is exploited as a tool to design and analyze switching controllers for cycling.

Learning control techniques, such as iterative learning control (ILC) and repetitive learning control (RLC), have been developed to improve tracking performance for repetitive or periodic systems by using control inputs from previous trials, iterations, cycles, or periods (Arimoto, Kawamura, & Miyazaki, 1984; Bristow, Tharayil, & Alleyne, 2006). ILC and RLC have been extensively applied for tracking of nonlinear systems to ensure asymptotic convergence and boundedness of the learning inputs (Dixon, Zergeroglu, Dawson, & Costic, 2002; Messner, Horowitz, Kao, & Boals, 1991; Sun, Ge, & Mareels, 2006). Moreover, learning control techniques have been utilized in several FES studies for upper body rehabilitation (Freeman, Rogers, Hughes, Burridge, & Meadmore, 2012). Spatial iterative learning methods have been developed to address the fact that many tracking tasks are not periodic in the time domain, but rather state periodic (Liu, Dong, Huang, & Yu, 2017; Moore, Ghosh, & Chen, 2007; Xu & Huang, 2008). Hence, spatial learning control could be utilized to track a desired torque trajectory based on crank position to evoke torque within favorable regions of the crank cycle.

In this paper and in our preliminary work in Duenas, Cousin, Ghanbari, and Dixon (2018), torque and cadence controllers are designed for FES-cycling power tracking. The motivation is to design a switched FES controller with spatial learning control to allow muscles to track a desired state-periodic torque trajectory on a stationary recumbent cycle. The muscle spatial learning controller is updated based on the crank position and acts as a feedforward input in contrast to high-gain/high-frequency control inputs that are prone to exacerbate muscle fatigue. A sliding-mode controller is designed for the electric motor to achieve cadence tracking and provide robustness to disturbances and uncertainties. The muscle and motor controllers are designed using a cycle-rider model that includes the effects of switching across muscle groups based on the rider's kinematic effectiveness. A passivity-based analysis is developed to ensure stability of the closed-loop torque and cadence error subsystems. The main benefit of using a passivity-based approach is that the motor controller complies to the muscle input, which acts as a disturbance in the closed-loop cadence tracking error, rather than rejecting it. Canceling the human input is not desirable due to the differences in the bandwidth of the muscle and motor controllers and uncertainty in the muscle dynamics. Experiments were conducted on five able-bodied individuals and three participants with NCs to assess the feasibility of the control technique. The combined average cadence tracking error for a 50 revolutions per minute (RPM) trajectory and power tracking error for a peak power of 10 W were 0.01 ± 1.20 RPM and 1.78 ± 1.25 W, respectively.

2. Cycle-rider dynamic model

The stationary cycle-rider system is modeled with the following dynamics (Bellman et al., 2016)

$$\tau_c(\dot{q},\ddot{q}) + \tau_r(q,\dot{q},\ddot{q},t) = \tau_e(t), \tag{1}$$

where $q:\mathbb{R}_{\geq t_0}\to\mathcal{Q}$ denotes the positive clockwise measurable crank angle, $\mathcal{Q}\subseteq\mathbb{R}$ denotes the set of crank angles, and $t_0\in\mathbb{R}$ is the initial time; $\tau_c:\mathbb{R}^2\to\mathbb{R}$ denotes the net cycle torque defined as $\tau_c(\dot{q},\ddot{q}) \triangleq J_c\ddot{q} + c_d\dot{q}$, where $J_c, c_d\in\mathbb{R}_{>0}$ denote the cycle's inertia and coefficient of viscous damping, respectively; $\tau_r:\mathcal{Q}\times\mathbb{R}^2\times\mathbb{R}_{\geq t_0}\to\mathbb{R}$ denote the rider torque applied about the crank; and $\tau_e:\mathbb{R}_{\geq t_0}\to\mathbb{R}$ is the electric motor torque applied about the crank defined as $\tau_e(t)\triangleq B_e u_e(t)$, where $B_e\in\mathbb{R}_{>0}$ satisfies $B_e\geq c_e\in\mathbb{R}_{>0}$, and $u_e:\mathbb{R}_{\geq t_0}\to\mathbb{R}$ is the motor current control input. The rider torque τ_r in (1) is defined as

$$\tau_r(q,\dot{q},\ddot{q},t) = \tau_p(q,\dot{q},\ddot{q},t) - \tau_a(q,\dot{q},t), \tag{2}$$

where $\tau_p:\mathcal{Q}\times\mathbb{R}^2\times\mathbb{R}_{\geq t_0}\to\mathbb{R}$ denotes the passive torque applied by the rider defined as $\tau_r\triangleq M_r(q)\ddot{q} + V(q,\dot{q})\dot{q} + G(q) + P(q,\dot{q})$, where $M_r:\mathcal{Q}\to\mathbb{R}_{>0}$ denotes the inertial effects of the rider, $V:\mathcal{Q}\times\mathbb{R}\to\mathbb{R}$ and $G:\mathcal{Q}\to\mathbb{R}$ denote the centripetal-Coriolis, and gravitational effects, respectively, $P:\mathcal{Q}\times\mathbb{R}\to\mathbb{R}$ denotes the effects of passive viscoelastic tissue forces in the rider's joints, and $\tau_a:\mathcal{Q}\times\mathbb{R}\times\mathbb{R}_{\geq t_0}\to\mathbb{R}$ denotes the active torque produced by muscle contractions and is defined as

$$\tau_a(q,\dot{q},t)\triangleq\sum_{m\in\mathcal{M}} B_m(q,\dot{q})u_m(t), \tag{3}$$

where $B_m:\mathcal{Q}\times\mathbb{R}\to\mathbb{R}_{>0}$, $\forall m\in\mathcal{M}$ represents the uncertain nonzero control effectiveness of each muscle group,[1] which depends on the unknown relationship between the stimulation intensity and the muscle group's evoked force, and the torque transfer ratios about the crank axis (Bellman et al., 2016). A muscle's stimulation intensity denoted as $u_m:\mathbb{R}_{\geq t_0}\to\mathbb{R}$ is applied in regions of the crank cycle where the joint torque transfer ratios are above a predefined threshold. Switching across muscles based on kinematic effectiveness yields an autonomous, state-dependent, switched control system. The portion of the crank cycle over which a particular muscle group is stimulated is denoted by $\mathcal{Q}_m\subset\mathcal{Q}$, $\forall m\in\mathcal{M}$, where the muscle groups are activated so that $\mathcal{Q}_M\triangleq\cup_{m\in\mathcal{M}}\mathcal{Q}_m$ (Bellman et al., 2016). A piecewise constant switching signal is developed for each muscle group, $\sigma_m\in\{0,\ 1\}$, $\forall m\in\mathcal{M}$ as $\sigma_m(q)\triangleq\begin{cases}1 & \text{if } q\in\mathcal{Q}_m\\ 0 & \text{if } q\notin\mathcal{Q}_m.\end{cases}$ The stimulation intensity to the muscle groups is defined as

$$u_m(t)\triangleq k_m\sigma_m u_{FES}, \tag{4}$$

where $k_m\in\mathbb{R}_{>0}$, $\forall m\in\mathcal{M}$ are selectable positive control gains, and $u_{FES}:\mathbb{R}_{\geq t_0}\to\mathbb{R}$ is a subsequently designed muscle input. The dynamic model in (1) can be rearranged using the definitions of the electric motor torque, the rider torque in (2), the active torque in (3), and (4) as

$$\begin{aligned}&M(q)\ddot{q} + V(q,\dot{q})\dot{q} + G(q)\\ &\quad + P(q,\dot{q}) + c_d\dot{q} + d(t) = B_\sigma u_{FES} + B_e u_e,\end{aligned} \tag{5}$$

[1] The subscript m indicates a muscle group contained in the muscle set $\mathcal{M}$.

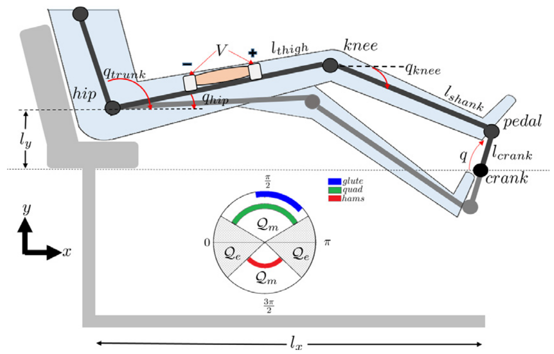

Fig. 1. Cycle-rider system schematic. The crank angle q and the net torque applied about the crank are positive in the clockwise direction. The knee, hip, and trunk angles are denoted by q_{knee}, q_{hip}, and q_{trunk}, respectively. The lengths of the thigh, shank, cycle crank, and horizontal and vertical seat positions are denoted by l_{thigh}, l_{shank}, l_{crank}, and l_x and l_y, respectively. The regions $\mathcal{Q}_m$ and $\mathcal{Q}_e$ denote the crank angles where the muscles and motor are active, respectively.

where $M : \mathcal{Q} \to \mathbb{R}_{>0}$ denotes the combined inertial effects of the rider and cycle defined as $M \triangleq J_c + M_r$, $d : \mathbb{R}_{\geq t_0} \to \mathbb{R}$ denotes the disturbances applied by the rider and unmodeled effects in the system, and $B_\sigma \in \mathbb{R}_{>0}$ is the lumped, switched control effectiveness defined as

$$B_\sigma(q,\dot{q}) \triangleq \sum_{m\in\mathcal{M}} B_m(q,\dot{q}) k_m \sigma_m(q). \tag{6}$$

The subscript $\sigma \in \mathcal{P} \triangleq \{1,2,3,\ldots,n\}$, $\mathcal{P} \subset \mathbb{N}$, $n \in \mathbb{N}$ indicates the index of B_σ, which switches according to the crank position. The sequence of switching states $\{q_n\}$ are known and the corresponding sequence of switching times $\{t_n\}$ are unknown and defined such that each t_n denotes the instant when q reaches the corresponding switching state q_n. The switching signal σ_m is assumed to be continuous from the right and designed to produce forward pedaling only. Fig. 1 shows a schematic of the cycle-rider system and illustrates the switching regions for the muscles and motor. The following assumption and properties from Bellman et al. (2016) are exploited in the subsequent control design and stability analysis.

Assumption 1. The disturbance d is bounded as $|d| \leq \xi_d$, where $\xi_d \in \mathbb{R}_{>0}$ is a known constant.

Property 1. *$c_m \leq M \leq c_M$, where c_m, $c_M \in \mathbb{R}_{>0}$ are known constants.*

Property 2. *$|V| \leq c_V\,|\dot{q}|$, where $c_V \in \mathbb{R}_{>0}$ is a known constant.*

Property 3. *$|G| \leq c_G$, where $c_G \in \mathbb{R}_{>0}$ is a known constant.*

Property 4. *$|P| \leq c_{P1} + c_{P2}\,|\dot{q}|$, where c_{P1}, $c_{P2} \in \mathbb{R}_{>0}$ are known constants.*

Property 5. *$\frac{1}{2}\dot{M} - V = 0$ by skew symmetry.*

Property 6. *The lumped switching control effectiveness is bounded as $c_b \leq B_\sigma \leq c_B$, $\forall\sigma \in \mathcal{P}$, where $c_b, c_B \in \mathbb{R}_{>0}$ are known constants.*

3. Control development

3.1. Cadence control

The first objective is to design a motor controller that tracks a desired cadence trajectory. The measurable angular crank position tracking error $e : \mathbb{R}_{\geq t_0} \to \mathbb{R}$ and auxiliary tracking error $r : \mathbb{R}_{\geq t_0} \to \mathbb{R}$ are defined as

$$e(t) \triangleq q(t) - q_d(t), \tag{7}$$

$$r(t) \triangleq \dot{e}(t) + \alpha e(t), \tag{8}$$

where $q_d : \mathbb{R}_{\geq t_0} \to \mathbb{R}$ denotes the desired crank position and its first two time derivatives are bounded (i.e., $|\dot{q}_d(t)| \leq \xi_1$ and $|\ddot{q}_d(t)| \leq \xi_2$, where $\xi_1, \xi_2 \in \mathbb{R}_{>0}$ are known) and $\alpha \in \mathbb{R}_{>0}$ is a constant control gain. After taking the time derivative of (8) and premultiplying by M, substituting for (5) and (7) and then performing some algebraic manipulation yield[2]

$$M\dot{r} = -Vr + \chi + \tilde{N} + B_\sigma u_{FES} + B_e u_e - e, \tag{9}$$

where the auxiliary signals $\chi : \mathbb{R}_{\geq t_0} \to \mathbb{R}$ and $\tilde{N} : \mathbb{R}_{\geq t_0} \to \mathbb{R}$ are defined as

$$\begin{aligned} \chi \triangleq\; & W_d - M(q)(\ddot{q}_d - \alpha\dot{e}) - V(q,\dot{q})(\dot{q}_d - \alpha e) - G(q) \\ & - P(q,\dot{q}) - c_d\dot{q} + N_d + e, \end{aligned} \tag{10}$$

$$\tilde{N} \triangleq -(W_d + N_d + d), \tag{11}$$

and the signals $W_d : \mathbb{R}_{\geq t_0} \to \mathbb{R}$ and $N_d : \mathbb{R}_{\geq t_0} \to \mathbb{R}_{>0}$ are defined as $W_d \triangleq M(q_d)\ddot{q}_d + V(q_d,\dot{q}_d)\dot{q}_d + G(q_d) + c_d\dot{q}_d$ and $N_d \triangleq c_{P1} + c_{P2}\dot{q}_d$, respectively. The auxiliary signal in (11) can be upper bounded as

$$|\tilde{N}| \leq \Theta_1, \tag{12}$$

where $\Theta_1 \in \mathbb{R}_{>0}$ is a known positive constant. By using Properties 1–4, (7), (8), and the Mean Value Theorem, an upper bound for (10) can be developed as

$$\chi \leq \rho(\|z\|)\|z\|, \tag{13}$$

where $z : \mathbb{R}_{\geq t_0} \to \mathbb{R}^2$ is defined as $z \triangleq [e\ \ r]^T$, and $\rho(\cdot) \in \mathbb{R}$ is a known positive, radially unbounded, nondecreasing function. Given the cadence open-loop error system in (9), the motor control input is designed as

$$u_e = -k_1 r - (k_2 + k_3\rho(\|z\|)\|z\|)\,\text{sgn}(r) + \nu_p, \tag{14}$$

where $k_1, k_2, k_3 \in \mathbb{R}_{>0}$ are selectable positive gain constants, $\text{sgn}(\cdot) : \mathbb{R} \to [-1, 1]$ is the signum function, and $\nu_p : \mathbb{R}_{\geq t_0} \to \mathbb{R}$ is a subsequently designed control input. The cadence motor control input in (14) includes a feedback term and robust control terms to reject the disturbance in (5) and the state-dependent function in (13). The closed-loop cadence error system is obtained by substituting (14) into (9) as

$$\begin{aligned} M\dot{r} =\; & -Vr + \chi + \tilde{N} + B_\sigma u_{FES} - e - B_e(k_1 r - \nu_p \\ & + (k_2 + k_3\rho(\|z\|)\|z\|)\,\text{sgn}(r)). \end{aligned} \tag{15}$$

3.2. Spatial learning control for torque tracking

The second objective is to track a desired torque trajectory in the muscle stimulation regions $q \in \mathcal{Q}_M$. The torque tracking error signal is designed based on the difference between the desired torque and an estimate of the active torque produced by the muscle contractions in (3). Torque sensors are commonly included on rehabilitation cycles, which provide a measurement of the net torque contributions about the crank. To obtain direct measurement of muscle force real-time invasive sensing is required, which is not practical. Similar to previous FES experiments (cf. Bellman, 2015; Ha et al., 2016), a baseline measurement of the required torque to drive the cycle-rider system at a desired cadence is obtained without applying FES (i.e., $\tau_a = 0$ such that $\tau_r = \tau_p$ in (2)) under the assumption that

[2] Functional dependencies are removed henceforth unless they add clarity to the exposition.

the disturbances are sufficiently small. By combining equations in (1) and (2), the dynamics can be expressed as

$$\tau_a + \tau_e = \tau_c + \tau_p. \tag{16}$$

A nominal torque measurement $\tau_n : \mathbb{R}_{\geq t_0} \to \mathbb{R}$ can be obtained from (16) as $\tau_n = \tau_e = \tau_c + \tau_p$ when FES is not applied (i.e., $\tau_a = 0$).

Assumption 2. An estimate of the nominal torque measurement $\hat{\tau}_n : \mathbb{R}_{\geq t_0} \to \mathbb{R}$ can be obtained using fitting techniques given continuous net torque measurements (Bellman, 2015). The mismatch between the nominal torque and the nominal torque estimate $\tilde{\tau}_n : \mathbb{R}_{\geq t_0} \to \mathbb{R}$ is defined as $\tilde{\tau}_n \triangleq \tau_n - \hat{\tau}_n \leq \epsilon_n$, where $\epsilon_n \in \mathbb{R}_{>0}$ is a known upper bound of the estimation error. This assumption is acceptable when FES is not applied (i.e., $\tau_a = 0$) during preliminary testing and if the desired cadence used in this test is the same as during the actual cycling experiment (Cousin et al., 2017).

Subtracting the nominal torque estimate $\hat{\tau}_n$ from both sides of (16) yields

$$\tau_a = \tilde{\tau}_n + \hat{\tau}_n - \tau_e. \tag{17}$$

Combining (17) with the estimate of the net active muscle torque $\hat{\tau}_a$ defined as $\hat{\tau}_a \triangleq \hat{\tau}_n - \tau_e$ yields

$$\hat{\tau}_a = \tau_a - \tilde{\tau}_n. \tag{18}$$

To quantify the torque control objective, an integral torque tracking error-like term $e_\tau : \mathbb{R}_{\geq t_0} \to \mathbb{R}$ is defined as

$$e_\tau = \int_{t_0}^{t} \left(\tau_d(\varphi) - \hat{\tau}_a(\varphi)\right) d\varphi, \tag{19}$$

where $\tau_d : \mathbb{R}_{\geq t_0} \to \mathbb{R}$ denotes a bounded periodic desired torque trajectory such that $|\tau_d| \leq \beta_d$.

Remark 1. In (19), the torque trajectory τ_d is a function of time. However in the experiments in Section 5, the desired torque trajectory τ_d is a bounded periodic function of the crank angle $q \in [0, 2\pi)$. Hence, a mapping between time and space is needed. This mapping is feasible since there exists a relationship between time and crank position. The angular speed of the system is defined as $\dot{q} \triangleq dq/dt$, which can be integrated to yield $q = \int_0^t \dot{q}(\varphi)d\varphi \triangleq f(t)$. In cycling only forward pedaling is allowed (no change of direction) and the desired cadence $\dot{q}_d$ is positive. Moreover, the cadence controller in (14) is designed and proven to achieve $\dot{q} > 0$ (i.e., the actual cadence is nonzero) based on the stability proof in Section 4. Hence, q is a strictly increasing function of t, (i.e., the relationship between t and q is bijective Xu & Huang, 2008). Thus the function $q = f(t)$ is analytic and the inverse function $t = f^{-1}(q)$ exists globally. Therefore, any function of t can be expressed as a spatial function of q, e.g., $\tau_d(t)$ can be expressed as $\tau_d(f^{-1}(q))$.

The torque open-loop error system is obtained by taking the time derivative of (19) and using (18), (3), (4), and (6) as

$$\dot{e}_\tau = \tau_d - B_\sigma u_{FES} + \tilde{\tau}_n. \tag{20}$$

Given the open-loop error system in (20), the muscle control input is designed as

$$u_{FES} = \hat{W}_d + k_4 e_\tau + k_5 \hat{W}_d, \tag{21}$$

where $k_4, k_5 \in \mathbb{R}_{>0}$ are positive constant control gains, and $\hat{W}_d : \mathbb{R}_{\geq t_0} \to \mathbb{R}$ is the subsequently designed RLC update law.

Remark 2. The RLC is typically designed based on the knowledge of the time period T of a periodic process (Dixon et al., 2002; Sun et al., 2006). In this paper, the RLC is designed based on the state periodicity (crank position) of the desired torque trajectory τ_d. Based on the mapping described in Remark 1, a spatial RLC denoted as $\hat{W}_d(t) = \hat{W}_d(f^{-1}(q))$ can be designed leveraging the fact that $q - 2\pi \triangleq f(t - T)$ and the existence of the map $t - T = f^{-1}(q - 2\pi)$. Knowledge of the period T (i.e., the time to complete a revolution) is not necessary for the implementation of $\hat{W}_d$, but it can be computed as $T = \int_{q-2\pi}^{q} dt = \frac{1}{\dot{q}} \int_{q-2\pi}^{q} dq$. The period T varies across crank cycles because it depends on the achieved cadence tracking performance.

The RLC update law in (21) is defined as

$$\begin{aligned} \hat{W}_d &\triangleq \Gamma \mathrm{sat}_{\beta_r}\left(\hat{W}_d(t - T)\right) + k_L e_\tau, \\ &= \Gamma \mathrm{sat}_{\beta_r}\left(\hat{W}_d(f^{-1}(q - 2\pi))\right) + k_L e_\tau, \end{aligned} \tag{22}$$

where $\Gamma \in (0, 1]$ is a selectable constant, $k_L \in \mathbb{R}_{>0}$ is a positive constant learning gain, and $\mathrm{sat}_{\beta_i}(\cdot)$ is defined as

$$\mathrm{sat}_{\beta_i}(\Xi) \triangleq \begin{cases} \Xi & \text{for } |\Xi| \leq \beta_i \\ \mathrm{sgn}(\Xi)\beta_i & \text{for } |\Xi| > \beta_i, \end{cases} \quad i \in \{d, r\},\ \forall \Xi \in \mathbb{R}. \tag{23}$$

where $\beta_i \in \mathbb{R}_{>0}$ are selectable constants satisfying $\beta_d < \beta_r$. The closed-loop error system is obtained by substituting (21) into (20) as

$$\dot{e}_\tau = \tilde{W}_d + \hat{W}_d + \tilde{\tau}_n - B_\sigma(\hat{W}_d + k_4 e_\tau + k_5 \hat{W}_d), \tag{24}$$

where $\tilde{W}_d : \mathbb{R}_{\geq t_0} \to \mathbb{R}$ is the learning estimation error defined as $\tilde{W}_d \triangleq \tau_d - \hat{W}_d$. Based on the periodicity and boundedness of τ_d, $\tau_d(t) = \mathrm{sat}_{\beta_d}(\tau_d(t)) = \mathrm{sat}_{\beta_d}(\tau_d(t - T))$. Hence, by exploiting (22), the following expression can be developed

$$\tilde{W}_d = \mathrm{sat}_{\beta_d}(\tau_d(t - T)) - \Gamma \mathrm{sat}_{\beta_r}(\hat{W}_d(t - T)) - k_L e_\tau(t). \tag{25}$$

4. Stability analysis

The stability of the RLC muscle and sliding-mode motor controllers can be examined independently through the following two theorems. Theorem 1 shows that the closed-loop torque error system is output strictly passive (OSP) and ensures asymptotic tracking or uniformly ultimately bounded (UUB) tracking provided two conditions, which hold for all time, are satisfied, respectively. Theorem 2 shows that the closed-loop cadence error system is OSP and exponential tracking is achieved for $q \notin \mathcal{Q}_M$ ensuring passivity with respect to the muscle input. Lemma 1 is used to prove that the time derivative of the torque tracking error in (19) is uniformly bounded.

Theorem 1. *The closed-loop error system in (24) is OSP from input v_1 to output e_τ if $q \in \mathcal{Q}_M$. The controller designed in (21) and RLC in (22) ensures asymptotic tracking if $\epsilon_n|e_\tau| > \epsilon_L$ in the sense that $\lim_{t\to\infty} e_\tau(t) = 0$ and UUB tracking if $\epsilon_n|e_\tau| < \epsilon_L$ in the sense that*[3]

$$|e_\tau| \leq \sqrt{\frac{\lambda_2}{\lambda_1}}|e_\tau(t_n)|e^{-\frac{\lambda_6}{2}(t-t_n)} + \sqrt{\frac{\lambda_5}{\lambda_1\lambda_6}}(1 - e^{-\frac{\lambda_6}{2}(t-t_n)}), \tag{26}$$

where $\lambda_1 \triangleq min(\frac{1}{2}, \frac{1}{2k_L})$, $\lambda_2 \triangleq max(\frac{1}{2}, \frac{1}{2k_L})$, $\lambda_5 \triangleq \frac{k_4 c_b \lambda_4}{\lambda_3} + \frac{2}{k_L}\epsilon_n^2$, and $\lambda_6 \triangleq \frac{k_4 c_b}{\lambda_3}$.

[3] For $q \notin \mathcal{Q}_M$ the torque controller in (21) and desired torque trajectory τ_d are zero.

Proof. Let $V_1 : \mathbb{R}^2 \times \mathbb{R}_{\geq t_0} \to \mathbb{R}$ be a nonnegative, continuously differentiable, storage function defined as

$$V_1 \triangleq \frac{1}{2}e_\tau^2 + \frac{1}{2k_L}\int_{t-T}^{t}(\mathrm{sat}_{\beta_d}(\tau_d(\varphi)) - \Gamma\mathrm{sat}_{\beta_r}(\hat{W}_d(\varphi)))^2 d\varphi. \tag{27}$$

The storage function in (27) satisfies the following inequalities:

$$\lambda_1\|w\|^2 \leq V_1(w,t) \leq \lambda_2\|w\|^2, \tag{28}$$

$$V_1(w,t) \leq \lambda_3\|e_\tau\|^2 + \lambda_4, \tag{29}$$

where $w \triangleq [e_\tau \;\; \sqrt{Q_L}]^T$, $Q_L \triangleq \int_{t-T}^{t}(\mathrm{sat}_{\beta_d}(\tau_d(\varphi)) - \Gamma\mathrm{sat}_{\beta_r}(\hat{W}_d(\varphi)))^2 d\varphi$, and λ_3, λ_4 are known positive bounding constants. Let $w(t)$ be a Filippov solution to the differential inclusion $\dot{w} \in K[h](w)$, where $K[\cdot]$ is defined as Filippov (1964) and h is defined using (24) as $h \triangleq [h_1 \;\; h_2]$, where $h_1 \triangleq \tilde{W}_d + \dot{\hat{W}}_d + \tilde{\tau}_n - B_\sigma(\hat{W}_d + k_4 e_\tau + k_5\hat{W}_d)$, $h_2 \triangleq \frac{1}{2\sqrt{Q_L}}\{(\mathrm{sat}_{\beta_d}(\tau_d(t)) - \Gamma\mathrm{sat}_{\beta_r}(\hat{W}_d(t)))^2 - (\mathrm{sat}_{\beta_d}(\tau_d(t-T)) - \Gamma\mathrm{sat}_{\beta_r}(\hat{W}_d(t-T)))^2\}$. The control input in (4) has the discontinuous lumped control effectiveness B_σ; hence the time derivative of (27) exists almost everywhere (a.e.), i.e., for almost all t. Based on Fischer, Kamalapurkar, and Dixon (2013, Lemma 1), $\dot{V}_1(w(t),t) \overset{a.e.}{\in} \dot{\tilde{V}}_1(w(t),t)$, where $\dot{\tilde{V}}_1$ is the generalized time derivative of (27) along the Filippov trajectories of $\dot{w} = h(w)$ and is defined as $\dot{\tilde{V}}_1 \triangleq \bigcap_{\xi\in\partial V_1}\xi^T K\left[\dot{e}_\tau \quad \frac{\dot{Q}_L}{2\sqrt{Q_L}} \quad 1\right]^T(e_\tau, 2\sqrt{Q_L}, t)$. Since $V_1(w,t)$ is continuously differentiable in w, $\partial V_1 = \{\nabla V_1\}$, thus $\dot{\tilde{V}}_1 \overset{a.e.}{\subset} [e_\tau, \left(\frac{1}{2k_L}\right)2\sqrt{Q_L}]K\left[\dot{e}_\tau \quad \frac{\dot{Q}_L}{2\sqrt{Q_L}}\right]^T$. Therefore, after substituting for (24), the generalized time derivative of (27) can be expressed as

$$\begin{aligned}\dot{\tilde{V}}_1 \overset{a.e.}{\subset}\; & e_\tau\left(\tilde{W}_d + \dot{\hat{W}}_d + \tilde{\tau}_n - K[B_\sigma](k_4 e_\tau + \hat{W}_d + k_5\hat{W}_d)\right)\\ & - \frac{1}{2k_L}(\mathrm{sat}_{\beta_d}(\tau_d(t-T)) - \Gamma\mathrm{sat}_{\beta_r}(\hat{W}_d(t-T)))^2\\ & + \frac{1}{2k_L}(\mathrm{sat}_{\beta_d}(\tau_d(t)) - \Gamma\mathrm{sat}_{\beta_r}(\hat{W}_d(t)))^2.\end{aligned} \tag{30}$$

By employing the following property

$$\left(\tau_d(t) - \hat{W}_d(t)\right)^2 \geq \left(\mathrm{sat}_{\beta_d}(\tau_d(t)) - \Gamma\mathrm{sat}_{\beta_r}(\hat{W}_d(t))\right)^2,$$

proven similarly as in Dixon et al. (2002, Appendix I) using $\beta_d < \beta_r$, using Property 6 to lower bound $K[B_\sigma]$, substituting for (25), and canceling terms, an upper bound for (30) can be developed as

$$\dot{\tilde{V}}_1 \overset{a.e.}{\leq} -\delta_1 e_\tau^2 + \upsilon_1 e_\tau, \tag{31}$$

where $\upsilon_1 = (1 + c_B - k_5 c_b)\hat{W}_d + \epsilon_n$, and $\delta_1 \triangleq c_b k_4 + \frac{k_L}{2}$. Integrating (31) yields $\int_{t_0}^{t}\upsilon_1(\varphi)e_\tau(\varphi)d\varphi \overset{a.e.}{\geq} \left(\tilde{V}_1(t) - \tilde{V}_1(t_0) + \int_{t_0}^{t}\delta_1 e_\tau^2(\varphi)d\varphi\right)$. Hence, the closed-loop system in (24) is OSP from input υ_1 to output e_τ. To ensure stability of the closed loop error system in (24), additional analysis is needed. The upperbound in (31) can be rewritten as

$$\dot{\tilde{V}}_1 \overset{a.e.}{\leq} -k_4 c_b e_\tau^2 + e_\tau\hat{W}_d(1 + c_B - k_5 c_b) + e_\tau\epsilon_n - \frac{1}{2}k_L e_\tau^2. \tag{32}$$

Selecting $k_5 \triangleq \frac{1+c_B}{c_b}$ and $k_L \triangleq \frac{2\epsilon_n^2}{\epsilon_L}$ and substituting them into (32) yields

$$\dot{\tilde{V}}_1 \overset{a.e.}{\leq} -k_4 c_b e_\tau^2 + \epsilon_n|e_\tau|\left(1 - \frac{1}{\epsilon_L}\epsilon_n|e_\tau|\right), \tag{33}$$

where asymptotic tracking is achieved if $\epsilon_n|e_\tau| > \epsilon_L$ and by invoking (Fischer et al., 2013, Corollary 2) and since $\dot{\tilde{V}}_1(w,t) \overset{a.e.}{\leq} -W(w)$, thus $|e_\tau| \to 0$ as $t \to \infty$, where W is a continuous positive semi-definite function. If $\epsilon_n|e_\tau| < \epsilon_L$, Eq. (33) yields

$$\dot{\tilde{V}}_1 \overset{a.e.}{\leq} -k_4 c_b e_\tau^2 + \epsilon_L \overset{a.e.}{\leq} -k_4 c_b e_\tau^2 + \frac{2\epsilon_n^2}{k_L}. \tag{34}$$

Further by using the inequality in (29), the inequality in (34) can be upperbounded as

$$\dot{\tilde{V}}_1 \overset{a.e.}{\leq} -\lambda_6 V_1 + \lambda_5, \tag{35}$$

where $\lambda_5 \triangleq \frac{k_4 c_b \lambda_4}{\lambda_3} + \frac{2}{k_L}\epsilon_n^2$ and $\lambda_6 \triangleq \frac{k_4 c_b}{\lambda_3}$. Applying the Comparison Lemma (Khalil, 2002, Lemma 3.4) to (35) yields

$$V_1(w) \overset{a.e.}{\leq} V_1(w(t_n))e^{-\lambda_6(t-t_n)} + \frac{\lambda_5}{\lambda_6}\left(1 - e^{-\lambda_6(t-t_n)}\right), \tag{36}$$

which can be used with (28) to yield the UUB tracking result in (26). Using (27) and (36), $V_1 \in \mathcal{L}_\infty$, hence, $e_\tau \in \mathcal{L}_\infty$. From (22), $\hat{W}_d \in \mathcal{L}_\infty$, which along with the fact that $\tau_d \in \mathcal{L}_\infty$ implies that $\tilde{W}_d \in \mathcal{L}_\infty$. From (21), $u_{FES} \in \mathcal{L}_\infty$, and from (4), $u_m \in \mathcal{L}_\infty$. A separate analysis is needed to prove that the time derivative of the torque tracking error in (19) $\dot{e}_\tau$ is bounded. The following lemma establishes a bound for $\dot{e}_\tau$.

Lemma 1. *The torque tracking error $\dot{e}_\tau$ in (24) is uniformly bounded for $q \in \mathcal{Q}_M$ in the sense that*

$$\begin{aligned}|\dot{e}_\tau| \leq\; & \left(2 + c_B\left(1 + \frac{k_4}{k_L} + k_5\right)\right)k_L|e_\tau|\\ & + \left(2 + \frac{\beta_d + \epsilon_n}{\Gamma\beta_r} + c_B(1 + k_5)\right)\Gamma\beta_r.\end{aligned} \tag{37}$$

Proof. The integral torque tracking error e_τ can be rewritten as

$$e_\tau = \int_{t_0}^{t}\frac{de_\tau(\varphi)}{d\varphi}d\varphi + C, \tag{38}$$

where $C \in \mathbb{R}$ is an integration constant. Based on (26), the expression in (38) can be used to prove that $\lim_{t\to\infty}\int_{t_0}^{t}\frac{de_\tau(\varphi)}{d\varphi}d\varphi$ exists and is finite. Using (23), (24), and (25), the upperbound for $|\dot{e}_\tau|$ in (37) can be obtained. Therefore, based on Theorem 1, $e_\tau, \hat{W}_d, \tilde{W}_d \in \mathcal{L}_\infty$, and hence $\dot{e}_\tau \in \mathcal{L}_\infty$.

Theorem 2. *The closed-loop cadence tracking error system in (15) is OSP from input υ_2 to output r. The controller in (14) achieves exponential tracking when $u_m = 0$, provided the following sufficient gain conditions are satisfied*

$$k_2 > \frac{\Theta_1}{c_e}, \quad k_3 > \frac{1}{c_e}. \tag{39}$$

Proof. Let $V_2 : \mathbb{R}^2 \times \mathbb{R}_{\geq t_0} \to \mathbb{R}$ be a nonnegative, continuously differentiable, storage function defined as

$$V_2 = \frac{1}{2}e^2 + \frac{1}{2}Mr^2. \tag{40}$$

The storage function in (40) satisfies $\lambda_7\|z\|^2 \leq V_2(z,t) \leq \lambda_8\|z\|^2$, where $\lambda_7 \triangleq \min(\frac{1}{2}, \frac{c_m}{2})$, $\lambda_8 \triangleq \max(\frac{1}{2}, \frac{c_M}{2})$. Let $z(t)$ be a Filippov solution to the differential inclusion $\dot{z} \in K[h](z)$, where $K[\cdot]$ is defined as in Fischer et al. (2013), and h is defined by using (7) and (8) as $h \triangleq [h_3 \;\; h_4]$, where $h_3 \triangleq r - \alpha e$ and $h_4 \triangleq M^{-1}\{-Vr + \chi + \tilde{N} + B_\sigma u_{FES} - e - B_e(k_1 r - \upsilon_p + (k_2 + k_3\rho(\|z\|)\|z\|)\,\mathrm{sgn}(r))\}$. Using similar arguments as in the proof of Theorem 1, using (12), (13), (15), and Properties 5 and 6, the generalized time derivative of (40) can be upper bounded as

$$\begin{aligned}\dot{\tilde{V}}_2 \overset{a.e.}{\leq}\; & -\alpha e^2 - k_1 c_e r^2 + \left(B_\sigma u_{FES} + c_e\upsilon_p\right)r\\ & - (k_2 c_e - \Theta_1)|r| - (k_3 c_e - 1)\rho(\|z\|)\|z\||r|.\end{aligned} \tag{41}$$

Table 1
Demographics of participants with a neurological condition.

Participant	Age	Sex	Injury	Months since injury
A	25	M	SB L5-S1	Since birth
B	32	M	SCI C5-C7, T12	76
C	28	F	MS	96

Integrating (41) yields $\int_{t_0}^{t} \upsilon_2(\varphi)r(\varphi)d\varphi \overset{a.e.}{\geq} (\tilde{V}_2(t) - \tilde{V}_2(t_0) + \int_{t_0}^{t} \delta_2\|z(\varphi)\|^2 d\varphi)$, where $\delta_2 = \min\{\alpha, k_1 c_e\}$, and $\upsilon_2 = B_\sigma u_{FES} + c_e \nu_p$, which can be used to prove that the closed-loop system in (15) is OSP from input υ_2 to output r, provided the sufficient gain conditions in (39) are satisfied. In fact, the system is strictly passive (Khalil, 2002) since the integral term in the right-hand side of passivity inequality is positive definite. Moreover, by setting $\nu_p \triangleq -k_p r$, $k_p \in \mathbb{R}_{>0}$ in (41), $\dot{V}_2 \overset{a.e.}{\leq} -\delta_3 V_2$ where $\delta_3 = \frac{\min\{\delta_2, k_p\}}{\lambda_8}$, during $q \notin \mathcal{Q}_M$ since $\sigma_m = 0 \implies B_\sigma = 0$, $\forall m \in \mathcal{M}$, provided the gain conditions in (39) are satisfied. Hence, exponential cadence tracking is obtained as $\|z(t)\| \leq \sqrt{\frac{\lambda_8}{\lambda_7}}\|z(t_n)\| \exp\left(-\frac{\delta_3}{2}(t - t_n)\right)$, $\forall q \notin \mathcal{Q}_M$.

5. Experiments

The controllers designed in (14), (21) and (22) were tested in experiments. The stimulation intensities u_m activated the right and left quadriceps (RQ, LQ), hamstrings (RH, LH), and gluteal (RG, LG) muscle groups for torque tracking, and the current input u_e was used for the electric motor to track cadence.

5.1. Participants

Five able-bodied individuals labeled as S1–S5 (three male and two female with age range of 22–26 years) and three individuals with NCs (one female with Multiple Sclerosis (MS) and two males with Spina Bifida and SCI) participated in the FES-cycling protocol. Demographics of the participants with NCs are listed in Table 1. The participants provided written informed consent as approved by the Institutional Review Board at the University of Florida and were instructed to avoid pedaling voluntarily.

5.2. Experimental testbed and setup

The cycling testbed described in Bellman et al. (2017) and Duenas et al. (2019) was used for experiments. The testbed has crank position and torque (SRM Science Road Wireless Power Meter) feedback. The motor was controlled using a current-controlled analog motor driver, a filter card, and a power supply (Advanced Motion Controls).[4] A desktop computer with Windows 10 OS, MATLAB/Simulink 2015b (MathWorks Inc) and QUARC 2.5 real-time software was used with a sampling frequency of 500 Hz. A Quanser Q8-USB data acquisition board measured the encoder and power meter signals and sent the voltage output to the motor driver. A current-controlled stimulator (RehaStim 1, Hasomed GmbH) delivered biphasic, symmetric, rectangular pulses to the muscle groups via self-adhesive PALS® electrodes (3″ by 5″).[5] The stimulation current amplitudes and frequency were selected as in Duenas et al. (2019). Measurements of the participant's legs were recorded as in Bellman et al. (2016) to compute the muscle stimulation regions.

[4] The servo drive and filter card were provided in part by the sponsorship of Advanced Motion Controls.

[5] Surface electrodes for the study were provided compliments of Axelgaard Manufacturing Co., Ltd.

The experiments included a warm up, a passive torque estimation trial and the main cycling trial. Warm up trials at different speeds with and without open-loop stimulation pulse trains were conducted for the participants with NCs to acclimate them to the cycle. An estimate of the nominal torque $\hat{\tau}_n$ was obtained in a separate trial where the muscles were not stimulated and the electric motor was used to passively rotate the participant's legs. The FES-cycling trial had a duration of $t_d = 180$ s. The electric motor tracked a time-varying cadence trajectory that reached a steady state value of 50 RPM after $t_1 = 16$ s. When the experiment duration reached $t_2 = 21$ s, the torque controller in (21) with RLC in (22) was activated and hence torque tracking started.

The desired torque trajectory was designed as a modified function of the knee joint torque transfer ratio, which can be computed as a function of the crank position. Therefore, the state-periodic desired torque trajectory is nonzero during the stimulation regions $q \in \mathcal{Q}_M$ and is defined as

$$\tau_d(q) \triangleq \begin{cases} A_d \sin\left(2\frac{q-q_1}{\frac{1}{2}q_2 - q_1}\pi\right) & q_1 < q \leq \frac{1}{2}q_2 \\ \frac{A_d}{2}\cos\left(\frac{q-\frac{1}{2}q_2}{\frac{1}{2}q_2}\pi\right) + \frac{A_d}{2} & \frac{1}{2}q_2 < q \leq q_2 \\ 0 & q_2 < q \leq q_3 \\ A_d \sin\left(\frac{q-q_3}{q_4-q_3}\pi\right) & q_3 < q \leq \frac{q_4+q_3}{2} \\ \frac{A_d}{2}\cos\left(\frac{q-\frac{1}{2}(q_4-q_3)+q_3}{\frac{1}{2}(q_4-q_3)}\pi\right) & \\ +\frac{A_d}{2} & \frac{q_3+q_4}{2} < q \leq q_4 \\ 0 & q_4 < q \leq q_1, \end{cases}$$

where $q_1, q_3 \in \mathbb{R}_{>0}$ and $q_2, q_4 \in \mathbb{R}_{>0}$ are the known and constant predefined crank angles that determine the start and the end of the stimulation regions, respectively. The peak torque amplitude $A_d \in \mathbb{R}_{\geq 0}$ is defined as $A_d \triangleq \frac{P_d}{\dot{q}_d}$, where $P_d \triangleq 10$ W, is the maximum desired power demand (unless stated otherwise), and $\dot{q}_d$ is the desired cadence. Since the electric motor tracks cadence throughout the entire crank cycle (i.e., the motor advances the crank position in and out of the torque tracking regions), the spatial RLC, which is initialized to zero, can be implemented without enforcing the typical resetting condition before the start of a new crank cycle or period. The control gains introduced in (4), (14), (21), and (22) were selected as follows: $k_m \in [4.5, 5]$, $\alpha \triangleq 2.5$, $k_1 \triangleq 9$, $k_2 \triangleq 0.1$, $k_3 \triangleq 0.01$, $k_4 \in [60, 250]$, $k_5 \triangleq 0.5$, $k_p \triangleq 0.001$, $\Gamma \in [0.95, 1]$, and $k_L \in [25, 45]$.

5.3. Results

Table 2 summarizes the average of the cadence error (i.e., the time derivative of (7)), the average of the torque tracking error in (19), the average of the time derivative of (19), and the average power tracking error for $t \in [t_2, t_d]$ sec. The power tracking error can be computed as the difference between the active power output $P_a = \tau_a \dot{q}$ and the desired power output $P_D = \tau_d \dot{q}_d$. For data analysis and to account for the time-delayed nature of muscle activation, the actual torque error $\dot{e}_\tau$ was computed by averaging the active torque output τ_a within a time window of 100 ms after the stimulation inputs were applied and turned off. Fig. 2 illustrates the switched muscle control inputs, the desired and actual torque output, and the RLC input for participant S3 (as a common example) after 2 min of cycling. Fig. 3 shows the root-mean-squared error (RMS) of the cadence tracking error calculated over a moving time interval window of 12 s, and

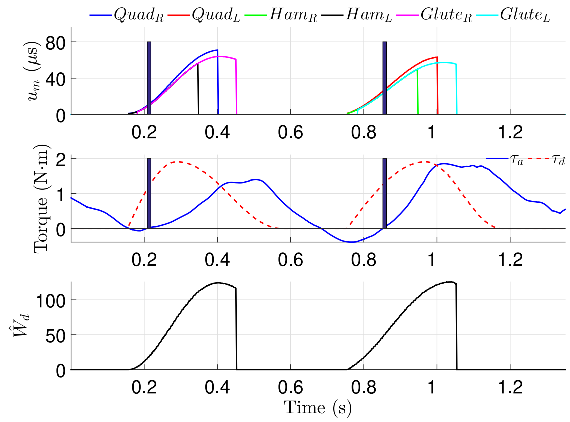

Fig. 2. FES intensities u_m (top), active torque output τ_a and desired torque τ_d (middle), and RLC input $\hat{W}_d$ (bottom) during a single crank cycle for participant S3 after 2 min of cycling. The vertical solid bars correspond to the time where the torque output rises above zero, which illustrates the fact that muscle activation is affected by the muscle electromechanical delay (EMD) (Downey, Merad, Gonzalez, & Dixon, 2017).

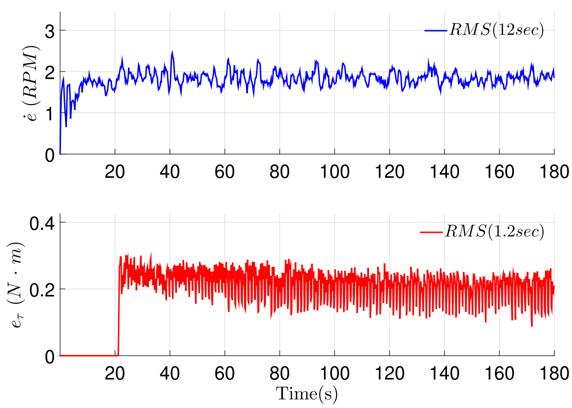

Fig. 3. Tracking performance for participant B quantified by the RMS cadence tracking error $\dot{e}$ computed with a moving time interval window of 12 s (top), and the RMS torque tracking error e_τ computed with a moving time interval window of 1.2 s (bottom).

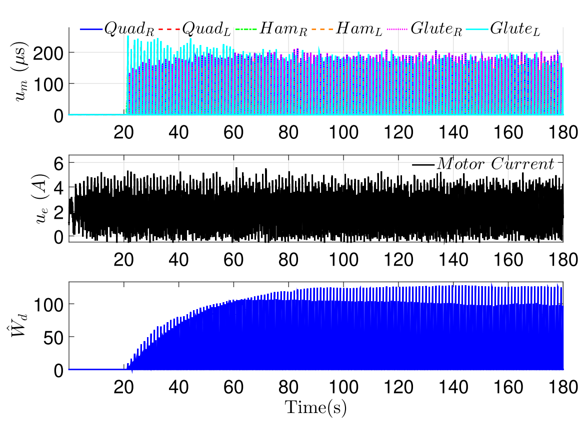

Fig. 4. Muscle stimulation intensities u_m (top), electric motor current u_e (middle), and RLC input $\hat{W}_d$ (bottom) for participant B.

the RMS of the torque tracking error calculated over a moving time interval window of 1.2 s for participant B. Fig. 4 depicts the muscle stimulation intensities u_m, the electric motor current input u_e, and the RLC input for participant B.

Table 2
Tracking results: average cadence tracking error $\dot{e}$, average torque error e_τ, average actual torque error $\dot{e}_\tau$ and the corresponding average power error reported as mean value ± standard deviation (STD).

Participant	$\dot{e}$ (RPM)	e_τ (N m s)	$\dot{e}_\tau$ (N m)	Power error (W)
S1	0.03 ± 1.07	0.08 ± 0.08	0.65 ± 0.24	3.41 ± 1.27
S2	0.01 ± 1.58	0.05 ± 0.12	0.24 ± 0.51	1.26 ± 2.56
S3	0.02 ± 0.85	0.10 ± 0.12	0.41 ± 0.30	2.15 ± 1.55
S4	0.02 ± 1.27	0.13 ± 0.18	0.31 ± 0.06	1.61 ± 0.32
S5	0.00 ± 0.96	0.12 ± 0.14	0.47 ± 0.18	2.45 ± 0.94
Mean (S1–S5)	**0.02 ± 1.17**	**0.10 ± 0.13**	**0.42 ± 0.30**	**2.18 ± 1.52**
A[a]	0.02 ± 0.68	0.04 ± 0.06	0.06 ± 0.03	0.30 ± 0.14
B	0.00 ± 1.78	0.06 ± 0.09	0.39 ± 0.19	2.11 ± 0.99
C[a]	0.01 ± 0.96	0.06 ± 0.10	0.18 ± 0.02	0.91 ± 0.13
Mean (A–C)	**0.01 ± 1.23**	**0.05 ± 0.09**	**0.21 ± 0.11**	**1.11 ± 0.58**
Combined mean	**0.01 ± 1.20**	**0.08 ± 0.12**	**0.34 ± 0.25**	**1.78 ± 1.25**

[a]Participants A and C tracked a peak power demand of $P_d = 5$ W.

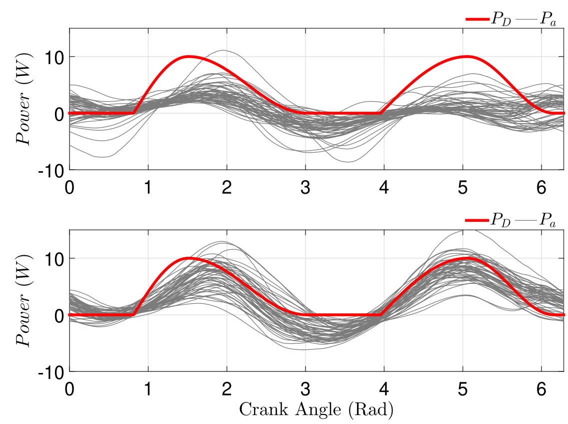

Fig. 5. Active power P_a and desired power P_d as a function of the crank angle for a trial with peak power $P_d = 10$ W and desired cadence $\dot{q}_d = 50$ RPM during the first 50 (top) and the subsequent 50 (bottom) crank cycles for participant S3.

Four trials were conducted for participant S3 to assess the effect of different cadences and peak power values. Table 3 summarizes the results of the four trials for participant S3 using $\dot{q}_d = 40$ RPM and $\dot{q}_d = 50$ RPM paired with $P_d = 5$ W and $P_d = 10$ W. Fig. 5 depicts the actual power output P_a and the desired power P_d as a function of the crank position for an experiment with peak power $P_d = 10$ W and desired cadence $\dot{q}_d = 50$ RPM during the first 50 crank cycles and the subsequent 50 crank cycles.

5.4. Discussion

The average cadence tracking errors were comparable between able-bodied participants (0.02±1.17 RPM) and individuals with NCs (0.01 ± 1.23 RPM). The average power tracking errors varied between healthy (2.18 ± 1.52 W) and impaired (1.11 ± 0.58 W) individuals, primarily due to the differences in muscle strength and desired peak torques. The muscle torque RLC controller improved the power tracking with increasing cycles as depicted in Fig. 5. The muscle and motor controllers were able to compensate for different peak torques and cadences, respectively, as reported in Table 3.

The results presented in this study align qualitatively with previously reported power tracking experiments. In Bellman (2015), three experimental results with healthy individuals were reported to track discrete power, where the power measurement was averaged over a full crank cycle and the controller was updated only at the beginning of the crank cycle. In Cousin et al.

Table 3
Tracking results using different peak power (P_d) and cadence ($\dot{q}_d$) values for participant S3: average cadence tracking error $\dot{e}$, average torque error e_τ, average actual torque error $\dot{e}_\tau$ and the corresponding average power error reported as mean value ± standard deviation (STD).

Cadence (RPM)	$\dot{e}$ (RPM)		e_τ (N m s)		$\dot{e}_\tau$ (N m)		Power error (W)	
	Peak power (W)		Peak power (W)		Peak power (W)		Peak power (W)	
	$P_d = 5$	$P_d = 10$	$P_d = 5$	$P_d = 10$	$P_d = 5$	$P_d = 10$	$P_d = 5$	$P_d = 10$
$\dot{q}_d = 40$	0.00 ± 0.69	0.01 ± 0.99	0.09 ± 0.10	0.11 ± 0.17	0.25 ± 0.19	0.02 ± 0.25	1.54 ± 1.29	0.88 ± 1.97
$\dot{q}_d = 50$	0.02 ± 0.91	0.02 ± 0.85	0.06 ± 0.06	0.10 ± 0.12	0.32 ± 0.18	0.41 ± 0.30	1.67 ± 0.95	2.15 ± 1.55
Mean	**0.01 ± 0.81**	**0.02 ± 0.92**	**0.08 ± 0.08**	**0.11 ± 0.15**	**0.29 ± 0.19**	**0.22 ± 0.28**	**1.61 ± 1.13**	**1.52 ± 1.77**

(2017), controllers were designed for muscles to track cadence and the electric motor to track a resistive torque. A closed-loop controller with motor assistance was reported in Hunt et al. (2004), where the power output was monitored for a paraplegic. In Farhoud and Erfanian (2014), a FES-cycling power control objective with varying amplitudes between 5 and 10 W was implemented with three paraplegics via sliding mode control. Despite the existing power tracking results, the lack of homogeneity in reporting the power tracking performance makes difficult the cross comparisons among the published results.

The implementation of the experiments presented several challenges. The active torque elicited by the participants was obtained by subtracting the nominal torque estimate from the net torque measurement. However, the noise in the nominal torque estimate of the rider's passive dynamics affected the quality of active torque signal. Future efforts should focus on improving the estimation of the rider's passive dynamics. Muscle fatigue and electromechanical delay (EMD) are two factors that degrade power tracking performance. Muscle fatigue is a well known issue in FES research and asynchronous stimulation patterns have been developed in Downey, Bellman, Kawai, Gregory, and Dixon (2015) to alleviate the effects of fatigue. However, muscle response to FES depends on the muscle activation dynamics, which is affected by EMD. As depicted in Fig. 2, there exists a muscle contraction delay illustrated by the time difference between the onset of the stimulation and the point where the participant's active torque rises above the zero torque baseline. Recently in Downey et al. (2017), it was concluded for the quadriceps that the EMD increases as the number of muscle contraction increases under isometric conditions. Hence, muscle fatigue and delay are important factors to consider for the development of rehabilitative treatments using FES.

The experiments with participants with NCs presented additional challenges. Participant B experienced muscle weakness, thus high stimulation intensities were needed to evoke muscle contractions, and suffered intermittent spasms that acted as disturbances. Participants A and C also exhibited reduced muscle strength, which lead to reduce the peak power from 10 W to 5 W. Moreover, participants A and C elicited asymmetric torque profiles between right and left legs. To compensate for torque asymmetries, a split-crank bicycle is an ideal testbed for further experimentation. Despite these challenges, the torque controller adjusted the muscle stimulation intensities to successfully complete the experiments. Clinical trials with populations with other NCs such as individuals with traumatic brain injury, Parkinson's disease, etc., are required to investigate the long-term benefits of the developed control methods.

6. Conclusion

A motor cadence controller and a muscle torque controller were implemented in this paper to achieve power tracking in FES-cycling experiments. The switched muscle torque controller included a spatial RLC input to cope with the state periodicity of the desired torque trajectory. A passivity-based analysis was developed to ensure stability of the torque and cadence closed-loop systems. The average cadence tracking error was 0.01±1.20 RPM and the average power tracking error was 1.78±1.25 W including all the participants. Muscle fatigue and the EMD are important factors that degrade the efficacy of the control methodology. As in results such as Downey et al. (2017), Merad, Downey, Obuz, and Dixon (2016) and Sharma, Gregory, and Dixon (2011), the muscle exhibits a delayed response to external electrical stimulation, and this response varies in time with muscle fatigue. Future efforts are required to develop controllers and analysis methods that can compensate for such delays in switched systems. Longitudinal studies are required to test the long-term benefits of learning control methods for power tracking.

References

Alibeji, N. A., Kirsch, N. A., & Sharma, N. (2015). A muscle synergy-inspired adaptive control scheme for a hybrid walking neuroprosthesis. *Frontiers in Bioengineering and Biotechnology*, *3*(203), 1–13.

Alibeji, N. A., Kirsch, N. A., & Sharma, N. (2017). An adaptive low-dimensional control to compensate for actuator redundancy and FES-induced muscle fatigue in a hybrid neuroprosthesis. *Control Engineering Practice*, *59*, 204–219.

Arimoto, S., Kawamura, S., & Miyazaki, F. (1984). Bettering operation of dynamic systems by learning: A new control theory for servomechanism or mechatronics systems. In *Proc. IEEE Conf. Decis. Control, Dec.* (pp. 1064–1069).

Bellman, M. (2015). *Control of cycling induced by functional electrical stimulation: a switched systems theory approach* (Ph.D. dissertation), University of Florida.

Bellman, M. J., Cheng, T. H., Downey, R. J., Hass, C. J., & Dixon, W. E. (2016). Switched control of cadence during stationary cycling induced by functional electrical stimulation. *IEEE Transactions on Neural Systems and Rehabilitation Engineering*, *24*(12), 1373–1383.

Bellman, M. J., Downey, R. J., Parikh, A., & Dixon, W. E. (2017). Automatic control of cycling induced by functional electrical stimulation with electric motor assistance. *IEEE Transactions on Automation Science and Engineering*, *14*(2), 1225–1234.

Bristow, D. A., Tharayil, M., & Alleyne, A. G. (2006). A survey of iterative learning control: a learning-based method for high performance tracking control. *IEEE Control Systems Magazine*, *26*(3), 96–114.

Cousin, C., Duenas, V. H., Rouse, C., & Dixon, W. E. (2017). Motorized functional electrical stimulation for torque and cadence tracking: A switched lyapunov approach. In *Proc. IEEE Conf. Decis. Control* (pp. 5900–5905).

Dixon, W. E., Zergeroglu, E., Dawson, D. M., & Costic, B. T. (2002). Repetitive learning control: A lyapunov-based approach. *IEEE Transactions on Systems, Man and Cybernetics, Part B (Cybernetics)*, *32*, 538–545.

Downey, R. J., Bellman, M. J., Kawai, H., Gregory, C. M., & Dixon, W. E. (2015). Comparing the induced muscle fatigue between asynchronous and synchronous electrical stimulation in able-bodied and spinal cord injured populations. *IEEE Transactions on Neural Systems and Rehabilitation Engineering*, *23*(6), 964–972.

Downey, R., Merad, M., Gonzalez, E., & Dixon, W. E. (2017). The time-varying nature of electromechanical delay and muscle control effectiveness in response to stimulation-induced fatigue. *IEEE Transactions on Neural Systems and Rehabilitation Engineering*, *25*(9), 1397–1408.

Duenas, V. H., Cousin, C., Ghanbari, V., & Dixon, W. E. (2018). Passivity-based learning control for torque and cadence tracking in functional electrical stimulation (FES) induced cycling. In *Proc. Am. Control Conf.* (pp. 3726–3731).

Duenas, V. H., Cousin, C. A., Parikh, A., Freeborn, P., Fox, E. J., & Dixon, W. E. (2019). Motorized and functional electrical stimulation induced cycling via switched repetitive learning control. *IEEE Transactions on Control Systems Technology*, *27*(4), 1468–1479.

Farhoud, A., & Erfanian, A. (2014). Fully automatic control of paraplegic FES pedaling using higher-order sliding mode and fuzzy logic control. *IEEE Transactions on Neural Systems and Rehabilitation Engineering*, *22*(3), 533–542.

Ferrante, S., Pedrocchi, A., Ferrigno, G., & Molteni, F. (2008). Cycling induced by functional electrical stimulation improves the muscular strength and the motor control of individuals with post-acute stroke. *European Journal of Physical and Rehabilitation Medicine*, *44*(2), 159–167.

Filippov, A. F. (1964). Differential equations with discontinuous right-hand side. In *ser. American mathematical society translations - Series 2*: *vol. 42*, *Fifteen papers on differential equations* (pp. 199–231). American Mathematical Society.
Fischer, N., Kamalapurkar, R., & Dixon, W. E. (2013). LaSalle-Yoshizawa corollaries for nonsmooth systems. *IEEE Transactions on Automatic Control*, *58*(9), 2333–2338.
Freeman, C. T., Rogers, E., Hughes, A.-M., Burridge, J. H., & Meadmore, K. L. (2012). Iterative learning control in health care: Electrical stimulation and robotic-assisted upper-limb stroke rehabilitation. *IEEE Control Systems Magazine*, *32*(1), 18–43.
Ha, K. H., Murray, S. A., & Goldfarb, M. (2016). An approach for the cooperative control of FES with a powered exoskeleton during level walking for persons with paraplegia. *IEEE Transactions on Neural Systems and Rehabilitation Engineering*, *24*(4), 455–466.
Hunt, K. J., Stone, B., Negård, N.-O., Schauer, T., Fraser, M. H., Cathcart, A. J., et al. (2004). Control strategies for integration of electric motor assist and functional electrical stimulation in paraplegic cycling: Utility for exercise testing and mobile cycling. *IEEE Transactions on Neural Systems and Rehabilitation Engineering*, *12*(1), 89–101.
Kawai, H., Bellman, M., Downey, R., & Dixon, W. E. (2019). Closed-loop position and cadence tracking control for FES-cycling exploiting pedal force direction with antagonistic bi-articular muscles. *IEEE Transactions on Control Systems Technology*, *27*(2), 730–742.
Khalil, H. K. (2002). *Nonlinear systems* (3rd ed.). Upper Saddle River, NJ: Prentice Hall.
Lew, B., Alavi, N., Randhawa, B. K., & Menon, C. (2016). An exploratory investigation on the use of closed-loop electrical stimulation to assist individuals with stroke to perform fine movements with their hemiparetic arm. *Frontiers in Bioengineering and Biotechnology*, *4*, 20.
Li, P. Y., & Horowitz, R. (1997). Control of smart exercise machines-part i: Problem formulation and nonadaptive control. *IEEE/ASME Transactions on Mechatronics*, *2*(4), 237–247.
Liu, J., Dong, X., Huang, D., & Yu, M. (2017). Composite energy function-based spatial iterative learning control in motion systems. *IEEE Transactions on Control Systems Technology*, *PP*(99), 1–8.
Merad, M., Downey, R. J., Obuz, S., & Dixon, W. E. (2016). Isometric torque control for neuromuscular electrical stimulation with time-varying input delay. *IEEE Transactions on Control Systems Technology*, *24*(3), 971–978.
Messner, W., Horowitz, R., Kao, W.-W., & Boals, M. (1991). A new adaptive learning rule. *IEEE Transactions on Automatic Control*, *36*(2), 188–197.
Moore, K. L., Ghosh, M., & Chen, Y. Q. (2007). Spatial-based iterative learning control for motion control applications. *Meccanica*, *42*(2), 167–175.
Nataraj, R., Audu, M. L., & Triolo, R. J. (2017). Restoring standing capabilities with feedback control of functional neuromuscular stimulation following spinal cord injury. *Medical Engineering & Physics*, *42*, 13–25.
Rouse, C., Duenas, V. H., Cousin, C., Parikh, A., & Dixon, W. E. (2018). A switched systems approach based on changing muscle geometry of the biceps brachii during functional electrical stimulation. *IEEE Control Systems Letters*, *2*(1), 73–78.
Sadowsky, C. L., Hammond, E. R., Strohl, A. B., Commean, P. K., Eby, S. A., Damiano, D. L., et al. (2013). Lower extremity functional electrical stimulation cycling promotes physical and functional recovery in chronic spinal cord injury. *The Journal of Spinal Cord Medicine*, *36*(6), 623–631.
Sharma, N., Gregory, C., & Dixon, W. E. (2011). Predictor-based compensation for electromechanical delay during neuromuscular electrical stimulation. *IEEE Transactions on Neural Systems and Rehabilitation Engineering*, *19*(6), 601–611.
Sun, M., Ge, S. S., & Mareels, I. M. (2006). Adaptive repetitive learning control of robotic manipulators without the requirement for initial repositioning. *IEEE Transactions on Robotics*, *22*(3), 563–568.
Szecsi, J., Straube, A., & Fornusek, C. (2014). Comparison of the pedalling performance induced by magnetic and electrical stimulation cycle ergometry in able-bodied subjects. *Medical Engineering & Physics*, *36*(4), 484–489.
Xu, J.-X., & Huang, D. (2008). Spatial periodic adaptive control for rotary machine systems. *IEEE Transactions on Automatic Control*, *53*(10), 2402–2408.
Zhang, J., & Cheah, C. C. (2015). Passivity and stability of human–robot interaction control for upper-limb rehabilitation robots. *IEEE Transactions on Robotics*, *31*(2), 233–245.

Victor H. Duenas received his M.S. and Ph.D. in 2016 and 2018, respectively, from the Department of Mechanical and Aerospace Engineering from the University of Florida, Gainesville, FL. In July 2018, he joined the Department of Mechanical and Aerospace Engineering at Syracuse University as an Assistant Professor. His research interests include nonlinear and adaptive control, rehabilitation robotics, cyber–physical systems, neuromuscular control, and human–robot interaction.

Christian A. Cousin joined the department of mechanical engineering at The University of Alabama as a faculty member in July 2019 after graduating with his doctorate from the University of Florida. He was awarded a National Science Foundation Graduate Research Fellowship in the spring of 2016 and his research interests include nonlinear and adaptive control, switched and hybrid systems, cyber-physical systems, hybrid exoskeletons, functional electrical stimulation, human-robot interaction, rehabilitation, and machine learning.

Vahideh Ghanbari received her M.S. and Ph.D. from the Department of Electrical Engineering at the University of Notre Dame in 2013 and 2017, respectively. In her Ph.D., her research focused on nonlinear control of switched and hybrid systems with applications to medical robotics.

Emily J. Fox, DPT, Ph.D., NCS is a Research Assistant Professor in the Department of Physical Therapy at the University of Florida and the Director of Neuromuscular Research at Brooks Rehabilitation. Her research focuses on neuromuscular control and functional recovery following neurologic injury or disease. A primary focus of her work is to develop and investigate innovative approaches such as electrical stimulation to enhance motor function and recovery.

Warren E. Dixon received his Ph.D. in 2000 from the Department of Electrical and Computer Engineering from Clemson University. He worked as a research staff member and Eugene P. Wigner Fellow at Oak Ridge National Laboratory (ORNL) until 2004, when he joined the University of Florida in the Mechanical and Aerospace Engineering Department, where he is an Ebaugh Professor. His main research interest has been the development and application of Lyapunov-based control techniques for uncertain nonlinear systems. Notable recognitions of his research include: the 2015 & 2009 American Automatic Control Council (AACC) O. Hugo Schuck (Best Paper) Award, the 2013 Fred Ellersick Award for Best Overall MILCOM Paper, the 2011 American Society of Mechanical Engineers (ASME) Dynamics Systems and Control Division Outstanding Young Investigator Award, the 2006 IEEE Robotics and Automation Society (RAS) Early Academic Career Award, an NSF CAREER Award (2006–2011). He is an ASME Fellow and IEEE Fellow.